Deposition of CdSe nanocrystals in highly porous SiO_2 matrices – in-situ growth vs. infiltration methods

Raktim Baruah [1,2], Munira Dilshad [2], Marco Diegel [2], Jan Dellith [2], Jonathan Plentz [2], Andreas Undisz [3,4], Adriana Szeghalmi [5,6] and Maria Wächtler [1,2*]

[1] Department of Chemistry and State Research Center OPTIMAS, RPTU Kaiserslautern-Landau, Erwin-Schrödinger-Str. 52, 67663 Kaiserslautern, Germany; raktim.baruah@rptu.de, maria.waechtler@chem.rptu.de

[2] Leibniz Institute of Photonic Technology, (Leibniz IPHT), Albert-Einstein-Str. 9, 07745, Jena, Germany; marco.diegel@leibniz-ipht.de; jan.dellith@leibniz-ipht.de; Jonathan.plentz@leibniz-ipht.de

[3] Institute of Materials Science and Engineering, Chemnitz University of Technology, Erfenschlager Str. 73, 09125 Chemnitz, Germany; andreas.undisz@mb.tu-chemnitz.de

[4] Otto Schott Institute of Material Research, Metallic Materials, Friedrich Schiller University Jena, 07743 Jena, Germany;

[5] Institute of Applied Physics, Friedrich Schiller University Jena, Albert-Einstein-Str. 15, 07745 Jena, Germany;

[6] Fraunhofer Institute for Applied Optics and Precision Engineering, Albert-Einstein-Str, 7, 07745, Jena, Germany; adriana.szeghalmi@iof.fraunhofer.de

[*] Correspondence: maria.waechtler@chem.rptu.de

Abstract: Embedding quantum dots into porous matrices is a very beneficial approach for generating hybrid nanostructures with unique properties. In this contribution we explore strategies to dope nanoporous SiO_2 thin films made by atomic layer deposition and atomic etching with precise control over pore size with CdSe quantum dots. Two distinct strategies were employed for quantum dot deposition: in-situ growth of CdSe nanocrystals within the porous matrix via successive ionic layer adsorption reaction, and infiltration of pre-synthesized quantum dots. To address the impact of pore size layers with 10 nm and 30 nm average pore diameter were used as matrix. Our results show that though potentially also small pores are accessible for the in-situ approach, this strategy lacks controllability over the nanocrystal quality and size distribution. To dope layers with high quality quantum dots with well-defined size distribution and optical properties infiltration of preformed quantum dots is much more promising. It was observed that due to higher pore volume 30 nm porous silica shows higher loading after treatment than 10 nm porous silica matrix. This can be related to a better accessibility of the pores with higher pore size. The amount of infiltrated QDs can be influenced via drop casting of additional solvent on a pre-drop casted porous matrix as well as via varying the soaking time of a porous matrix in a QD solution. Luminescent QDs deposited via this strategy keep their luminescent properties upon deposition and the resulting thin films with immobilized quantum dots are suited for integration into optoelectronic devices.

Keywords: CdSe quantum dots; thin film; porous silica

1. Introduction

Semiconductor nanocrystals (NCs) have emerged as the pivotal material in nanotechnology for the applications in optoelectronics, sensing and biomedical imaging, owing to their unique size-dependent optoelectronic properties.[1] Among them, quantum dots (QDs) stand out for their excellent and wide-ranging optical and electronic properties, which can be adjusted by varying their size. As the size of the QD is reduced, discrete quantized energy levels are observed in contrast to the continuous energy band structure observed in bulk materials.[2,3] This phenomenon is a consequence of the strong spatial confinement of electron and hole motion when the QD size is below the Bohr radius.[2,3] One of the most extensively studied system are CdSe QDs. CdSe QDs exhibit narrow photoluminescence spectra and can be designed to show high photoluminescence quantum yields (PLQY), and are therefore highly suitable for device applications such as in light-emitting diodes (LEDs)[4-6] or in sensing[7,8] applications. The tunability of electronic properties via size allows for the optimization of the valence band and conduction band energy levels allowing emission color, or to ensure sufficient driving force for energy and electron transfer processes forming the basis for sensing[7-9] concepts or the applications of QDs as light absorbers to drive photocatalytic reactions.[10-12] The synthesis of high quality (with respect to crystallinity and control over size distribution) CdSe QDs is achieved via the well-established hot injection method.[13,14] QDs resulting from this synthetic approach are usually capped with long-chain aliphatic surface ligands, e.g., tri-octylphosphine oxide, octadecylphosphonic acid, oleic acid, hexadecylamine etc.[15] The surface ligands provide colloidal stability, stabilize the surface of the QDs and saturate dangling bonds which are the source of surface trap states or introduce additional trapping states, depending on the anchoring functional group of the surface ligand.[16-18] Surface functionalization can also alter the dispersibility of the QDs in different solvents, rendering them suitable for applications in various solvent environments, e.g., in aqueous environments for sensing in biological systems[7] or photocatalytic applications[12,19] in aqueous environments.

The colloidal solutions of the QDs have the advantage to allow for solution processing, e.g., to generate thin films with controlled homogeneity, and packing density enabling fine tuning of optoelectronic properties and allowing for much more flexibility and large scale processing compared to methods such as chemical vapour deposition, epitaxial growth etc.[20,21] For many applications, dispersed NCs have to be transferred into thin film architectures, e.g., for application in LEDs[22,23], materials for photovoltaic devices[24-26], photoelectrode materials for photocatalytic[27] applications and sensors[28], or optoelectronic devices[29] for detection of radiation. Beyond thin film production by deposition of particles on substrates, immobilization and thin film production by integration of QDs into porous matrices, e.g., mesoporous silica, is a very interesting approach. The porous matrices support ordered assembly controlled by the structure of the porous matrix,[30] can be used to control size[31] via pore sizes of the matrix serving as template. The porous matrix surrounding can shield the QDs from environmental factors such as oxygen and moisture and improve light extraction[32] reducing thermal effects leading to improving long term stability and efficiency, e.g., observed for LED devices.[31,33,34] Furthermore, porous matrices can support the targeted function by reduction of non-radiative recombination, contributing to improved quantum efficiency and brightness of the LEDs [35] or support charge carrier separation by co-immobilizing donors and acceptors reducing charge carrier transfer distances and enhancing photocatalytic performances.[36] Furthermore, it can facilitate efficient diffusion of reactants and products, leading to improved reaction rates and yields in photocatalytic processes in the confined surrounding of the pores.[37]

Two general strategies exist to deposit QDs inside a porous matrix. For direct generation of NCs within the porous material successive ionic layer adsorption and reaction (SILAR) approach can be used.[30,38,39] E.g., Besson et al.[30] and Wang et al.[39] demonstrate growth of CdS QDs and CdSe QDs, respectively, in porous silica matrices via in-situ growth of QDs inside the pores. Short immersion times and repeated cycles allow for control of loading and particle sizes, though with limited precision and broad size distributions..[30] To overcome the missing precision in controlling size and size distribution of NCs generated via the SILAR method within the porous matrices, infiltration of pre-synthesized particles employing methods with high control over size distributions can be employed. This approach has been used for depositing colloidal QDs inside mesoporous silica particles in the so called “wet mixing method”[33,34,40], but also was adapted porous silica layers by soaking[41] in a solution of dispersed QDs.
In this contribution, we investigate strategies for the incorporation of nanocrystalline CdSe into porous silica layers with pore diameters in the 10s of nm range produced via atomic layer deposition (ALD).[42] Fabrication methods based on ALD are shown to be advantageous with respect to control over thickness of the porous layer and rigidity of the porous structure compared to sol-gel methods.[43-45] Two general strategies are employed to deposit nanocrystalline CdSe into the porous material: in-situ growth of CdSe NCs using SILAR approach and infiltration of pre-synthesized QDs. Analysis of structure and optical properties of the thin films in dependence on experimental parameters, e.g., pore size and deposition times, is performed to evaluate the quality of the produced layers.

2. Materials and Methods

For the NC synthesis the following chemicals were used: Tri-octylphosphine oxide (TOPO, 99%), Trioctylphosphine (TOP, 97%), Cadmium oxide (CdO, 99.99%), Cadmium acetate hydrate ($Cd(OAc)_2$. xH_2O, 99.99%), Selenium (Se, 99.99%), Sodium selenide (Na_2Se, 95%), Toluene (99.8% anhydrous) and Methanol (99.8% anhydrous) were purchased from Sigma Aldrich and Octadecylphosphonic acid (ODPA, 97%) was purchased from Carl Roth.
CdSe QDs were synthesized following established protocols.[46,47] 60 mg of cadmium oxide (CdO), 0.28 g of octadecylphosphine oxide (ODPA) and 3.0 g of trioctylphosphine oxide (TOPO) were mixed in a 25 mL three neck flask. The mixture was heated to 80 °C under N_2 atmosphere until melting under stirring. A vacuum was applied to remove traces of water and after bubble formation had stopped the mixture was heated to 150°C and evacuated for 1h. Then, under N_2 flow, the reaction mixture was heated up and around 300 °C the solution became optically clear and colourless. At 320 °C, 1.5 g of trioctylphosphine (TOP) was injected into the solution. When the temperature reached 380 °C, a solution of TOP:Se (0.058 g Se dissolved in 0.360 g TOP) was injected and the temperature was kept at 370 °C for 5 min. Then the reaction mixture was cooled down by removing the heating mantel and when the temperature reached 60 °C 10 ml toluene was injected. After the synthesis, QDs were precipitated by adding 10 mL MeOH to the reaction mixture and centrifugation at 5300 rpm. The precipitate was redispersed in toluene and three more times repeatedly precipitated and redispersed for cleaning. Finally, the QDs were redispersed in 10 mL of toluene and stored inside glove box (N_2 atmosphere).
Nanoporous SiO_2 layers were prepared using the methods reported by Ghazaryan et al.[42] Briefly, a heterostructure of SiO_2:Al_2O_3 is deposited by atomic layer deposition (ALD) using a sequence of 2 cycles of SiO_2 and 3 or 4 cycles of Al_2O_3, respectively. The sequence was repeated 230 and 330 times, respectively. The growth rate of the

SiO2 and Al_2O_3 is about 0.1 nm/ cycle. The film thickness of the [2:3]x230 sample is 123 nm, and 230 nm for the [2:4]x330 sample as estimated by spectroscopic ellipsometry measurements. After deposition, the Al_2O_3 is selectively etched in H_3PO_4 (85%) solution and a porous SiO_2 matrix is formed. The maximum pore size as estimated by SEM was 10 nm and 30 nm, being smaller when less Al_2O_3 is removed from the SiO_2 matrix. Porous silica layers were prepared both on fused silica to enable optical characterization and on silicon substrates to perform electron microscopy for imaging.

QDs were grown in-situ in the pores of the silica matrix by the Successive Ionic Layer Adsorption Reaction (SILAR) method following a protocol described by Sankapal et al.[48] The porous silica layer (either on fused silica or silicon substrate) was immersed first into a $Cd(OAc)_2$ solution (40 mL $Cd(OAc)_2$ in methanol, 5 µM) for 5 minutes. After taking it out, the layer was rinsed with methanol and dried under vacuum. Then the layer was immersed into a Na_2Se solution (40 mL Na_2Se in methanol, 6 µM) for 5 minutes, followed by rinsing with methanol and drying under vacuum. This completes one cycle of immersion. The immersion procedure was repeated several times and layers were produced applying 5, 10, 15 and 20 immersion cycles.

To infiltrate pre-synthesized QDs into porous silica, two strategies were applied - drop casting of a QD solution on porous silica layer and immersion and soaking of porous silica layer in a QD solution. For drop casting, 100 µL of QD solution (3 µM, toluene) were dropped on porous silica layers. Once the solvents were completely evaporated the layers were rinsed with toluene to remove QDs just adsorbed at the surface and dried under vacuum. For some of the layers, after the initial dropcasting step using a solution of QDs, additional solvent was dropped on the substrates to wash QDs just sitting on the surface into the pores. Alternatively, the porous silica layers were immersed in 3 mL of QD solution (0.4 µM, toluene) to soak QDs into the pores. Soaking times of 0.5 h, 2 h and 24 h followed by rinsing with toluene and drying under vacuum were applied. For comparison and to proof infiltration into the porous structure, a normal glass substrate, cleaned by washing with acetone, methanol, Hellmanex and water, was drop casted with 100 µL of QD solution (3 µM, toluene) and one other normal glass substrate was immersed in a QD solution (0.4 µM, toluene) for 24 hr followed by washing with toluene.

UV-vis absorption spectroscopy in the wavelength range from 200 nm to 1000 nm was performed using a Jasco V-780 spectrophotometer. Colloidal dispersions were measured in a 1 cm quartz cuvette and for thin film measurements a special film holder was used. Absorption spectra measured in thin films contain strong wavelength dependent scattering contributions which were corrected via fitting a polynomial background as described in Figure S3.

Photoluminescence spectra of the QD solution was recorded in a 1 cm cuvette using a FLS 980 Edinburgh Instruments Fluorimeter upon excitation at 400 nm. Photoluminescence spectra of porous silica layers on fused silica were recorded using a Horiba Fluorolog-3. The excitation wavelength was set to 400 nm.

To determine the photoluminescence lifetimes, Time Correlated Single Photon Counting (TCSPC) was performed with a Horiba DeltaFlex spectrometer with a pulsed NanoLED (peak wavelength of 389 nm, pulse duration of 1.3 ns) from Horiba. For this, QD solution was prepared in a 1 cm quartz cuvette. QD thin film and porous layers were measured using a suitable thin film holder.

Transmission Electron Microscopy (TEM) images were recorded using a JEM-ARM200F NEOARM (Jeol) operating at 80 kV. For that Colloidal QDs were deposited on a carbon coated Cu grid (purchased from PLANO GmbH). To evaluate the average

size and size distribution of the particles the images were processed using ImageJ 1.53a program.[49]
Scanning Electron Microscopy (SEM) images of QDs deposited on silicon wafer and porous silica on silicon wafer were recorded using a JEOL JSM-6700F scanning electron microscope. Additionally, cross sectional images of the porous silica layers were collected after breaking the substrate and depositing a carbon layer.
For elemental analysis, Energy Dispersive X-ray Spectrometry (EDX) on porous silica layers on silicon wafers using a Bruker silicon drift detector SDD-5030 (30 mm^2 detector area) with 10 keV electron energy was performed. Grazing incidence X-ray diffraction (giXRD) on porous silica layers on fused silica was performed using a Panalytical X´Pert Pro MPD ((Cu-Kα radiation, 1.541 Å) with omega angle 2°, 2theta range from 10° to 90°, 0.026° step size and measuring times from 1h to 15h).
Secondary Ion Mass Spectrometry (SIMS) was performed using a Hiden Analytical SIMS Workstation equipped with 5keV5 keV Cesium and Oxygen ion sources for ionization and sputtering for the material within a spot of 50 µm and a high transmission quadrupole secondary ion mass spectrometer. A below 10 nm thin Pt layer was deposited on top for electrically conductive surfaces to prevent electrical charging during measurement.

3. Results and Discussions

Porous silica layers were prepared using atomic layer deposition (ALD) of a heterostructure of SiO_2:Al_2O_3, followed by selective etching of Al_2O_3.[42] In order to systematically investigate the extent of QD deposition applying different methods, porous layers with two different pore sizes were prepared. Top view and cross section SEM images of the porous layers are shown in Figure S1. Average pore sizes of 10 nm and 30 nm were determined from SEM images. The thicknesses of the layers are in the range from 123 nm and 230 nm.
The first preparation route applied was to grow CdSe NCs directly inside the porous matrix. For this, a SILAR protocol was adopted.[48] Methanolic solutions of $Cd(OAc)_2$ as Cd^{2+} source and Na_2Se as Se^{2-} source were used. 5 min immersion of the porous layer into $Cd(OAc_2)$ solution leads to a monolayer adsorption of Cd^{2+} ions attached to the porous surface via Van der- Waals and electrostatic forces. Loosely bound Cd^{2+} ions were removed by rinsing the porous layers before immersion into a Na_2Se solution, which initiates the reaction of Cd^{2+} and Se^{2-} to form CdSe. Further successive cycles of immersions of the porous layers into $Cd(OAc)_2$ and Na_2Se solutions lead to successive growth of CdSe NCs. To observe the growth in the successive immersion steps, samples were prepared with 5, 10, 15 and 20 immersions for both, the layers with 10 nm and 30 nm pore size.
Steady state UV-vis absorption spectroscopy was performed on the porous silica layers, which shows absorption features below 700 nm. With the number of immersion steps, the absorption feature is increasing in intensity and the onset of absorption is shifting to higher wavelengths. This indicates on the one hand increasing loading of the SiO_2 matrix with CdSe and on the other hand an increase of the crystal size of the CdSe deposited (Figure 2). Similar behaviour was observed upon in-situ growth of CdS NCs on TiO_2 via SILAR method.[48] Typically, CdSe QDs exhibit distinctive electronic transitions from the valence band to conduction band due to the presence of quantized energy levels at the band edges.[50] In contrast, here the absorption spectra show only very broad features without any distinct peak. This can be related to a broad size distribution caused by uncontrolled growth of CdSe crystals and aggregation of smaller NCs with increasing number of immersion cycles forming larger particles. The absorption features of the layers with 30 nm pore size exhibit a notable increase in

absorbance with the number of immersion cycles. In contrast, the absorption of the layers with 10 nm pore size show a pronounced rise from the initial immersions to 10 cycles, followed by a saturation. This suggests that the limited pore volume of 10 nm pore-sized layers is fully occupied by the NCs or narrow parts of the porous structure are clogged preventing further deposition of CdSe, while the 30 nm pore-sized layers continue to fill. No photoluminescence was detected from the layers. This potentially is due to low crystal quality, i.e., low crystallinity and a high density of the NCs grown via this method.

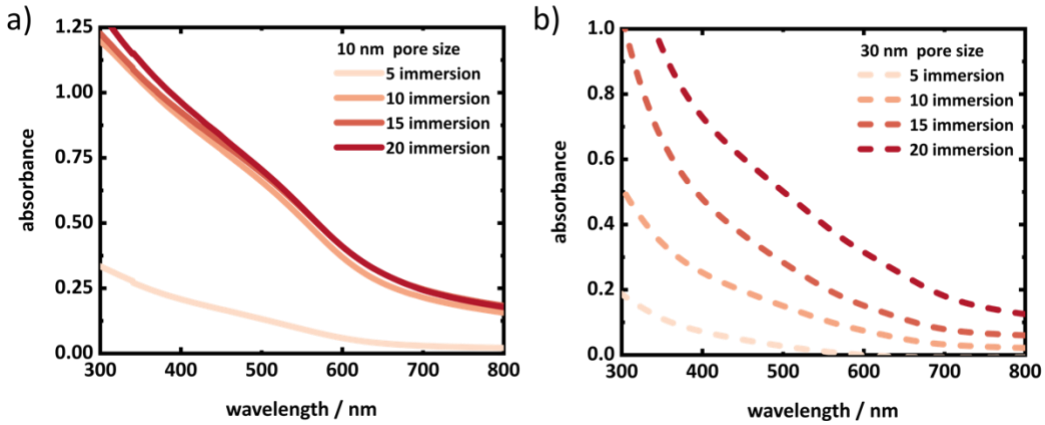

Figure 1. Absorption spectra of porous silica layers on fused silica substrates of (a) 10 nm and (b) 30 nm pore size with different numbers of SILAR immersion cycles. The absorption spectra of the thin films contain strong wavelength dependent scattering contributions. A correction for this scattering contribution as suggested in the supporting information **Figure S3**, cannot be performed reliably for these samples, because it is not possible to assign regions absorption due to the broad absorption feature, in the investigated spectral range.

To evaluate the crystal quality the samples were characterized by giXRD. **Figure 2** shows the giXRD patterns from porous silica layers with in-situ grown CdSe QDs. As the CdSe crystallites grown inside 10 nm and 30 nm pores are very small in size, the corresponding XRD peaks are broadened, but seem to grow in and sharpen with increasing immersion cycles.[51] The broad and less intense XRD peaks of CdSe NCs make it very challenging to distinguish between the cubic and hexagonal phases. However, conducting the in-situ growth at room temperature increases the likelihood of cubic crystal phase formation. From a thermodynamic perspective, the cubic phase is more stable at lower temperatures, while the hexagonal phase is more stable at higher temperatures.[51] It seems at least from the dataset of the sample with 30 nm pore size, that with the number of immersions, XRD peaks are evolving with potentially growing size of the embedded crystallites representing a cubic pattern with its characteristic 2 theta peaks at 24.84˚ (111) and 42.83˚ (220) (ICSD: 620421). Nevertheless, this conclusion needs to be regarded with care. On the other hand, due to smaller pore volume CdSe QDs grown in 10 nm pores must be smaller than in 30 nm pores, which is in good agreement with the XRD pattern, where the layers of 10 nm pore size show broader XRD peaks than the layers of 30 nm pore size.

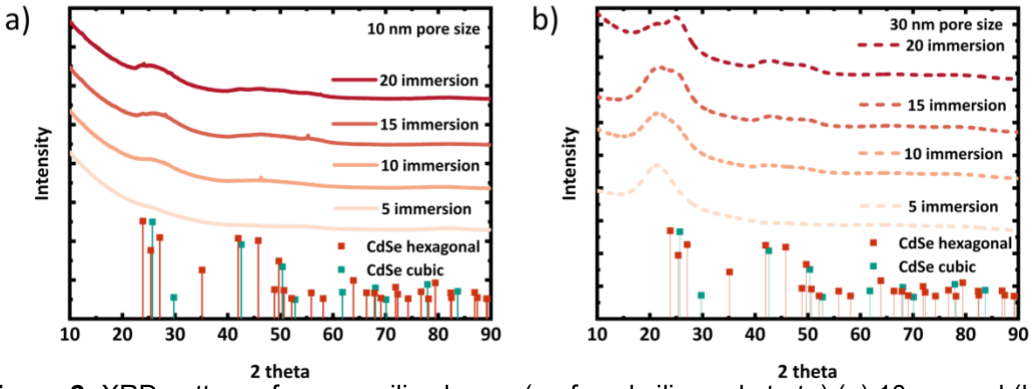

Figure 2: XRD pattern of porous silica layers (on fused silica substrate) (a) 10 nm and (b) 30 nm pore size with different number of SILAR immersion steps. The XRD patterns shown in the figure are without any background correction.

Further, to observe the CdSe QDs in the porous matrices, Energy Dispersive X-ray Spectrometry (EDX) was performed. **Figure 3** depicts the EDX spectra of 10 nm and 30 nm porous layers. While collecting EDX spectra, an area of 200 μm^2 was exposed to the electron beam. In comparison to spot analysis this large area exposure gives a good comparability among different samples lowering the danger of local overestimations. For both, the 10 nm and 30 nm pore-sized layers, there is a relative increase in the intensities of the Cd and Se peaks with the number of immersion cycles (**Figure 3**). The increasing Cd and Se peak intensities reflect the increasing amount of Cd and Se deposited in the layers with every SILAR immersion cycle.

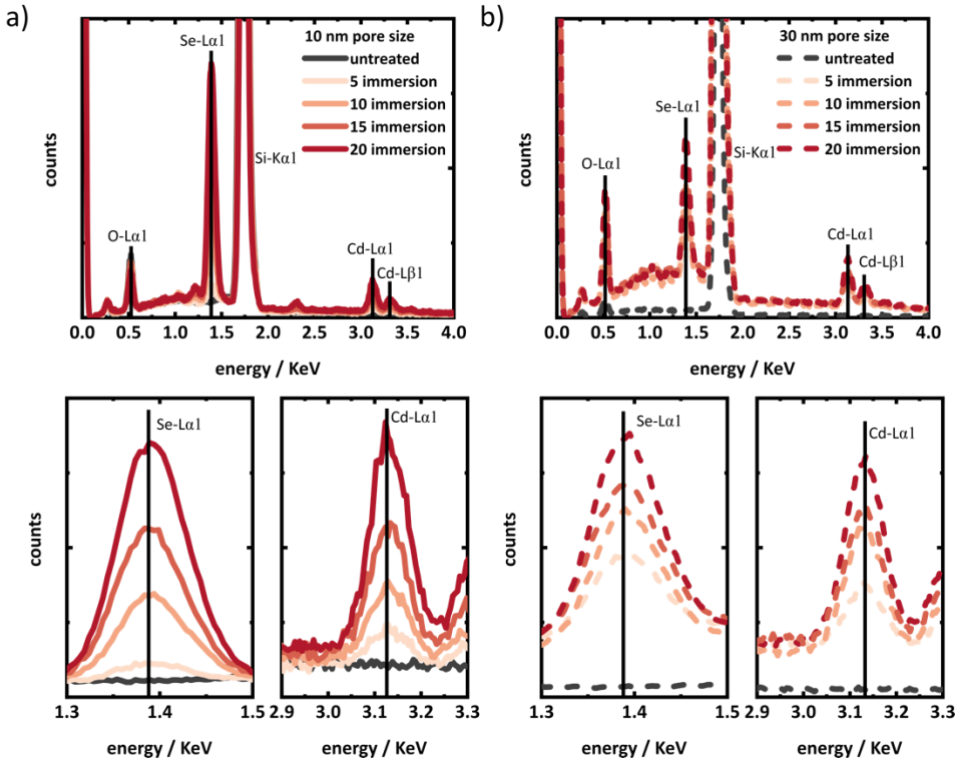

Figure 3: EDX spectra of porous silica layers (Si wafers) of (a) 10 nm and (b) 30 nm pore size with different SILAR immersions. Respective bottom panels show the zoomed regions of Se and Cd peaks.

SEM images of porous layers in silicon wafers were collected to observe the local structure of CdSe NCs in the porous structure. **Figure 4** and **Figure S8** depict the SEM images of 30 nm and 10 nm pore sized layers respectively. Because the resolution of SEM is not sufficient to image single NCs, which might be even more complex in case

of a broad size distribution, a clear presence of CdSe NCs cannot be confirmed from the top view image. Nevertheless, it appears from the top view images, that pores are gradually filling with increasing number of immersion cycles.

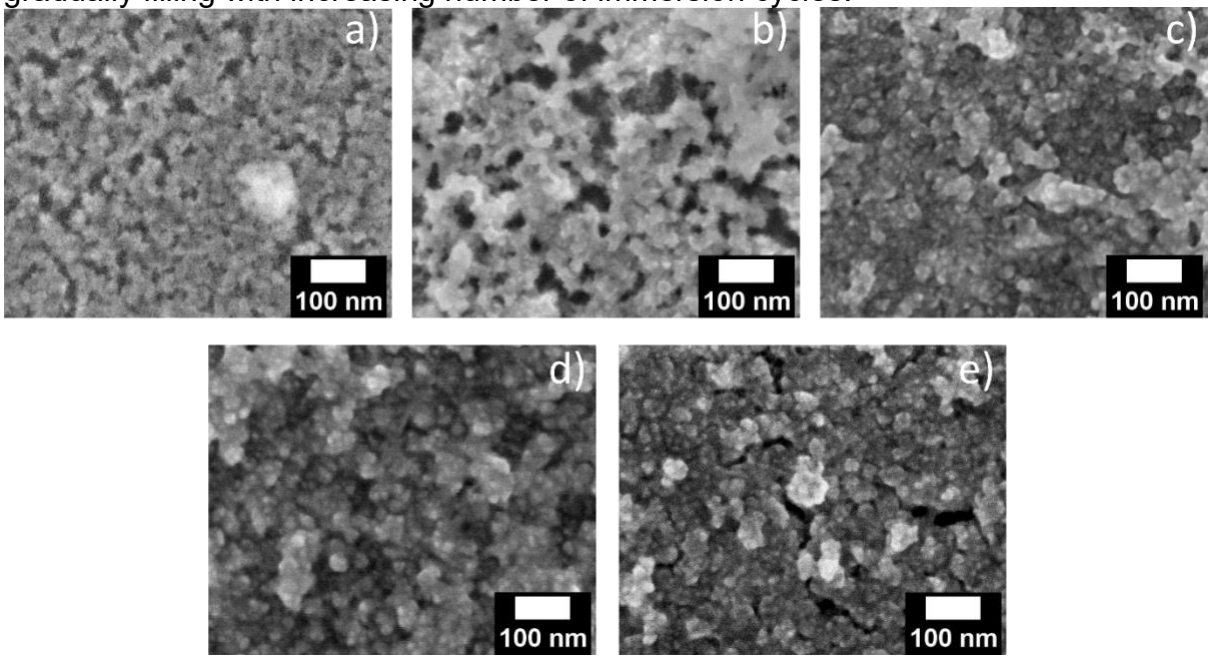

Figure 4: SEM images of (a) Untreated porous silica layers of 30 nm pore size in silicon wafer and with (b) 5, (c) 10, (d) 15 and (e) 20 SILAR immersions.

To summarize, the in-situ SILAR growth leads to the deposition of CdSe NCs on the porous matrix. Steady state absorption and photoluminescence spectroscopy, XRD and EDX analysis complemented by SEM imaging, indicates that the NCs are deposited probably within the porous network. However, the deposition at the surface cannot be ruled out and prevented. The NCs exhibit indications of a cubic phase with low crystallinity and a broad size distribution. Additionally, they demonstrate an absence of photoluminescence, which is likely related to the high number of trap states, which in turn decreases the PLQY. For any optoelectronic applications, it is essential to embed particles with better controllable properties, such as distinct electronic transitions, controllable size, and high crystalline NCs that support high PLQYs. The synthesis of highly crystalline CdSe NCs with a narrow size distribution via the SILAR method is a challenging process, necessitating the exploration of alternative strategies. These strategies must be capable of embedding NCs with high crystallinity and controllable properties, including a narrow size distribution. This leads us to seek an alternative porous silica and CdSe QD ensemble that exhibits superior performance, including a high PLQY, good crystallinity, and a narrow size distribution.

To achieve this goal, we employed an alternative method, which allows us to benefit from the well-controlled properties of colloidal QDs synthesized via hot-injection methods performed at high temperatures (usually > 300°C), resulting in CdSe QDs with precise control over size and size distribution, high crystallinity, high PLQY, narrow photoluminescence band width, etc.[14] However, such synthesis routes are typically not applicable to embed CdSe QDs directly during synthesis into porous silica layers due to the lack of thermal stability in that temperature range.[52] Additionally, the crystal growth in the hot injection method undergoes a fast nucleation mechanism,[14] which is hindered by the porous matrix, resulting in inefficient growth inside the pores. As this rules out the feasibility of employing the hot injection method for direct growth within the porous layer, we explore the possibility of deposition and infiltration of pre-synthesized QDs into the porous silica matrix.

For our study, CdSe QDs were pre-synthesized via hot injection (see experimental). [46,47] The QDs are majorly covered with TOPO as surface ligand along with TOP and ODPA (used with Se and Cd precursors in the QD synthesis) which make them dispersible in non-polar solvents like toluene, chloroform, and hexane etc. Absorption spectra of the pure QD dispersion (toluene) shows the characteristic electronic transition from valence band to conduction band states (**Figure 5a**). The feature at 537 nm corresponds to the lowest excitonic band edge $1S_{(e)}$-$1S_{3/2(h)}$ transition.[50] A band gap of the QDs of 2.2 ± 0.04 eV was derived from the Tauc's plot which is in agreement with the band edge photoluminescence peak position (547 nm, 2.26 eV).[53] The absolute PLQY is 3.9 %. The diameter of the QD was estimated from the spectral position of the lowest excitonic transition in the absorption spectra by the empirical formula derived by Peng et al.[54] to approximately 2.9 nm, in good agreement with the average diameter determined by statistical analysis of TEM images (3.2 ± 0.5 nm, **Figure S2** & **Figure 5b**). Furthermore, a thin film was prepared by drop-casting the QDs on a silicon wafer to visualize the QDs in layer via SEM (**Figure 5c**).
Pre-synthesized CdSe QDs were infiltrated into porous silica of pore size 10 nm and 30 nm via (a) drop casting of a QD solution (3 µM) in toluene on the porous silica layers and (b) soaking porous silica layers in a QD solution (0.4 µM) in toluene. We started with a simple drop casting followed by washing the layers with toluene to remove QDs sitting just on top of the surface. To induce higher infiltration of QDs, additional solvent (toluene) was dropped on the layers after the first step of drop casting followed by washing the layer in toluene. In the soaking method, porous layers were immersed in a QD solution. The loading of QDs was influenced by soaking time as described in the experimental section. Because of the surface ligand TOPO, QDs are hydrophobic. Therefore, in each washing step after infiltration, the QDs sitting on the hydrophilic porous layer surface should be effectively removed.

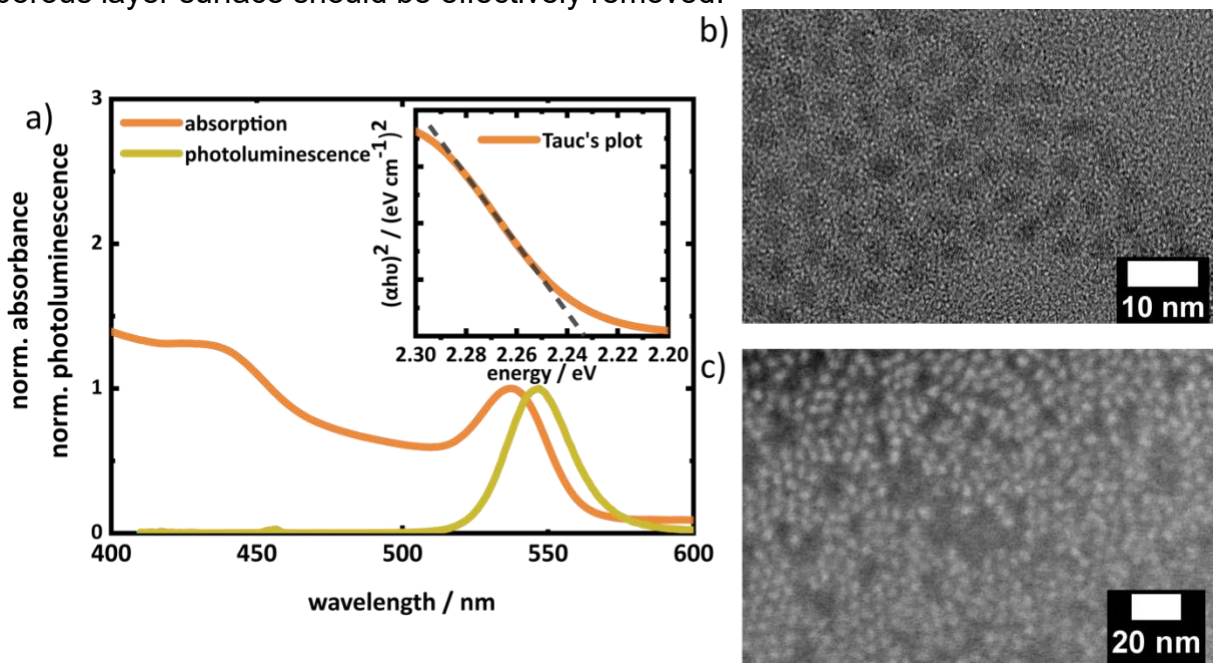

Figure 5: (a) normalized absorption and photoluminescence spectra (λ_{ex} 400 nm) of the CdSe QDs with 2.9 nm diameter in toluene, Tauc's plot for band gap calculation (inset). (b) TEM and (c) SEM image (on silicon wafer) of 2.9 nm CdSe QDs used in this study.

The deposition of pre-synthesized QDs on porous silica layers was confirmed by steady-state UV-VIS absorption spectroscopy and photoluminescence spectroscopy. **Figure 6** and **Figure S5** show the spectra of porous silica layers after QD infiltration. The absorption spectra were corrected for background signal from the substrate and

scattering contributions from the porous layer (see supplementary information **Figure S3**). The characteristic feature of the lowest band edge transition ($1S_{(e)}$-$1S_{3/2(h)}$) is clearly visible in the absorption spectra of the treated layers, which confirms the presence of QDs. After QD infiltration via both drop casting and soaking, for the porous layers with 30 nm pore size a higher absorbance is observed than for the layer with 10 nm pore size. This is an indication of a higher loading of QDs in bigger pores (i.e., 30 nm) than in 10 nm pores, which indicates an easier accessibility of the larger pores for the QDs. For the drop casting routine, treatment with additional solvent resulted in a relative increase compared to the drop casted layers without additional solvent treatment (**Figure 6a**). For the soaking strategy, the amount of QDs infiltrated into the pores increases with time of soaking. **T**he gradual increase of absorption of QDs in porous layers for soaking times 0.5 h to 2 h (**Figure S5a**) and 2 h to 24 h (**Figure 6c**) indicate the increase of the amount of infiltrated QDs. The band edge photoluminescence peak of the QDs at 541 nm in the photoluminescence spectra of the porous layers further confirms the presence of QDs in the treated porous layers. Due to inhomogeneous distribution of QDs and strong scattering contributions, quantitative comparison of both absorbance and photoluminescence intensity among samples is not possible. It can still be assumed that due to higher loading of QDs, porous silica layers of 30 nm pore size show higher photoluminescence intensity than the layer of 10 nm pore size for all infiltration methods (**Figure 6** and **Figure S5**). Similar to the absorption spectra, additional drop casting of toluene increases the photoluminescence intensity due to higher infiltration of QDs. On the other hand, the photoluminescence intensity also increases with soaking time (**Figure 6** and **Figure S5**).

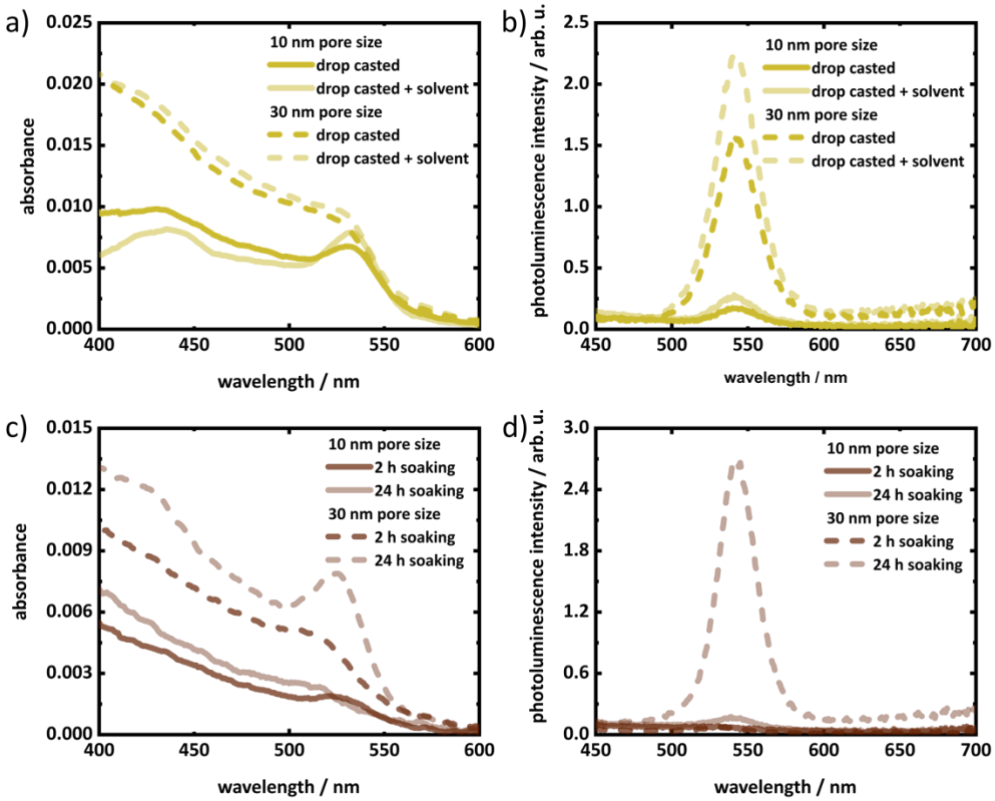

Figure 6: Absorption spectra (a) and photoluminescence spectra (b) of 10 nm (solid lines) and 30 nm (dashed line) porous layers treated by drop casting and drop casted followed by solvent treatment. Absorbance spectra (a) and photoluminescence spectra (b) of 10 nm (solid lines) and 30 nm (dashed line) porous layers with 2 h and 24 h soaking. The wavelength scattering correction as described in **Figure S3** was employed in the absorption spectra (a) and (c).

TCSPC was performed to investigate the changes in photoluminescence lifetime of QDs after infiltration into porous silica. **Figure 7** and **Figure S6** show the decay traces of pure QDs (in both solution and film) and the treated porous layers. These traces were modelled using a multiexponential function with three components, and the fitted data are presented in **Table S1**. The average photoluminescence lifetime was determined by amplitude weighted averaging of the time constants. The pure QD solution has an average lifetime of 38.7 ns, which is reduced to 19.2 ns when deposited on a glass substrate. This reduction is attributed to inter-QD interactions, such as non-radiative energy transfer within layer due to the inhomogeneous QD size distribution.[55-57] The photoluminescence decay of QD-infiltrated porous layers is also faster, as shown in **Table S1**. Porous layers with higher QD loading, as indicated by absorption and photoluminescence spectroscopy, exhibit faster photoluminescence decay. The average photoluminescence lifetime of the 30 nm drop-casted layers is 20.1 ns. However, with the addition of additional solvents, the lifetime decreases to 15.5 ns. Similarly, with increased soaking time, the photoluminescence lifetime of the 30 nm porous layer decreases from 17.8 ns to 11.7 ns. This trend is also observed for the 10 nm porous layers. It is expected that a higher loading of QDs will result in a denser packing inside the pores, leading to a stronger interaction between QDs. Therefore, the faster decay of photoluminescence in porous layers with higher QD loading is attributed to stronger interaction leading to enhanced non-deactivation. However, there is no significant difference in the photoluminescence lifetime in dependence of pore sizes.

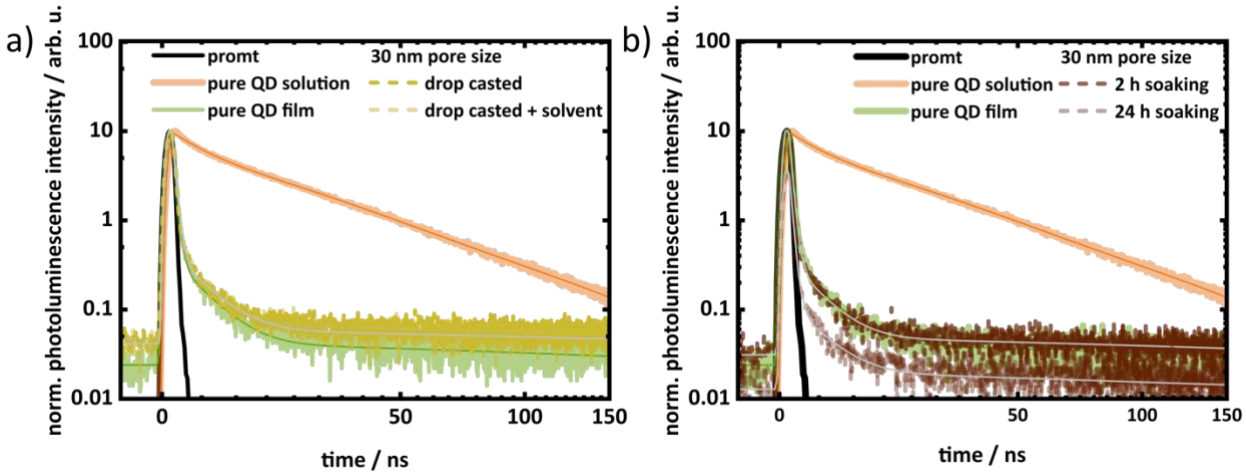

Figure 7: Decay kinetic traces of 30 nm porous layers with QD infiltration via (a) drop casting and (b) soaking along with the pure QD both in solution and thin film.

From steady state absorption and photoluminescence spectroscopy, we can only derive information on the presence of QDs on the substrates in general, but it is not possible to distinguish between QDs infiltrated in the pores or just sitting at the surface. An indication for infiltration is that after treating a glass substrate following the soaking method no QDs are deposited on the substrate (absorption spectra see supporting information (**Figure S10a)**. Similar behaviour was observed following the drop casting method where absorbance at the first excitonic peak is reduced by a factor of 6 after washing as depicted in **Figure S10b**. This indicates that QDs deposited on the surface get removed after the washing step of QD infiltration in porous layers, i.e., the spectra we are recording are from the QDs inside pores.

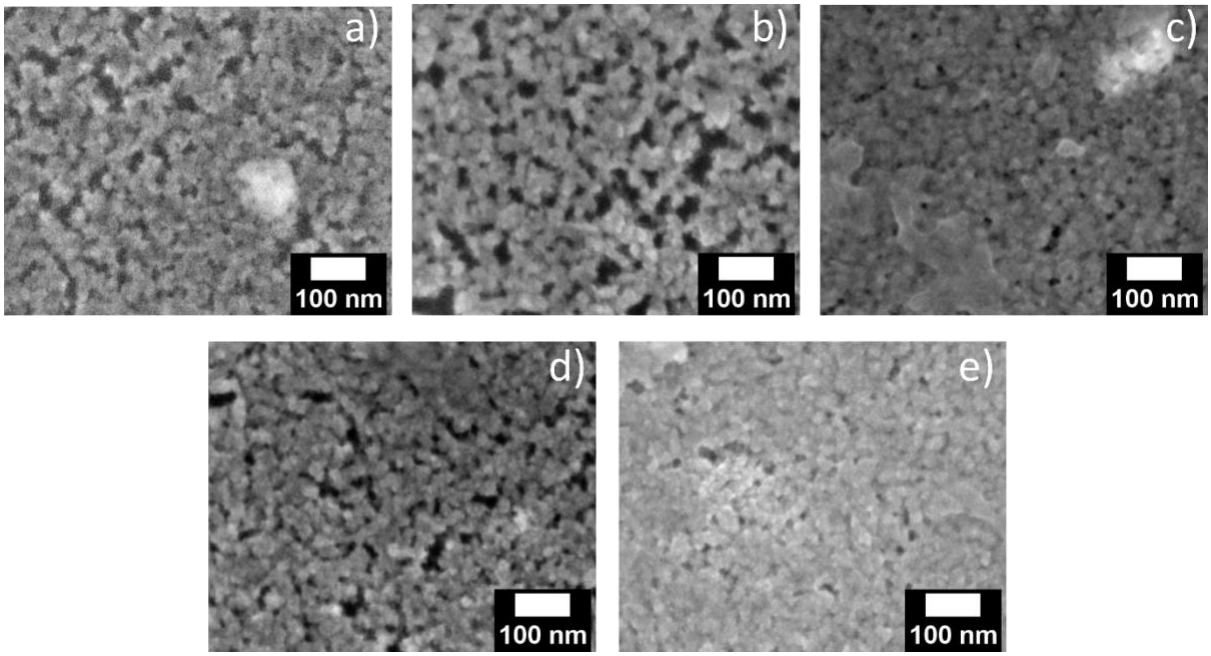

Figure 8: SEM images of (a) Untreated, (b) QD dropcasted, (c) QD drop casted + solvent, (d) soaked for 0.5 h and (e) soaked for 24 h, porous silica layers of 30 nm pore size in silicon wafer.

For further proof for the successful deposition of QDs inside the pores of the porous matrix, scanning electron microscopy (SEM) images were collected for porous layers on silicon substrates treated via the methods described above. Due to the insufficient contrast, it is difficult to localize QDs in the porous matrix in a top view image. Nevertheless, the opening of the pores at the surface of the structure (**Figure 8a**) seems to be smaller after infiltration (**Figure 8b, 8c, 8d & 8e**), which could be caused by QD infiltration and filling of the pores. **Figure 8b** and **8c** compares drop casted layer with a drop casted layer with additional solvent treatment, which indicates an increased pore filling after additional solvent treatment in agreement with the results from absorption and photoluminescence spectroscopy. On the other hand, porous structures are gradually filling with soaking time due to higher infiltration (**Figure 8d** & **8e)**. Similar behaviour was observed for 10 nm pore sized layers (**Figure S7**). Unfortunately, due to limited spatial resolution of the method, cross section images and EDX elemental mapping could not be collected to directly see the presence of QDs inside the porous layers.

To collect further proof for the presence of CdSe QDs inside the pores of the porous silica layers, Secondary Ion Mass Spectrometry (SIMS) was performed with a depth profile. The layer system of thin Pt film (for electrical non-charging) on porous layers on Si wafer were sputtered by an ion beam of the SIMS setup. The secondary ions generated from the material are recorded over the depth. A below 10 nm thin Platinum (Pt) layer was deposited on top of the porous layer for electrical non-charging and as indicator for when the porous layer structure is reached in the sputtering process. **Figure 9** shows the SIMS depth profile of a QD infiltrated porous silica layers of 30 nm pore size. Generated secondary ions from the porous layers are detected with respect to time (plotted in the X-axis) which is corelated to the depth of the layer. The region of interest in the SIMS depth profiles is between the two dashed lines which corresponds to the porous layer. As expected, the untreated porous layer does not contain Cd, that's why no signal was observed (**Figure 9 (a)**). **Figure 9 (b)** and **(c)** depict the presence of Cd in the porous layers. Even after washing the porous layers after infiltration there seems to be small amounts of QDs on the surface, which are seen in the early times

(before the dashed line at 1 min) as a less intense Cd signal. Further moving towards the depth of the porous layer Cd concentration gets higher which indicates that higher amount of Cd is present inside the porous layers, levelling off with increasing depth. Cd signal is finished once the sputtering reaches the Si wafer (dashed line at 6 min). Similar behaviour was observed for the layers of 10 nm pore sized layers (see supplementary material, **Figure S9**). The presence of CdSe QDs in the pores is ensured by the SIMS data shown above.

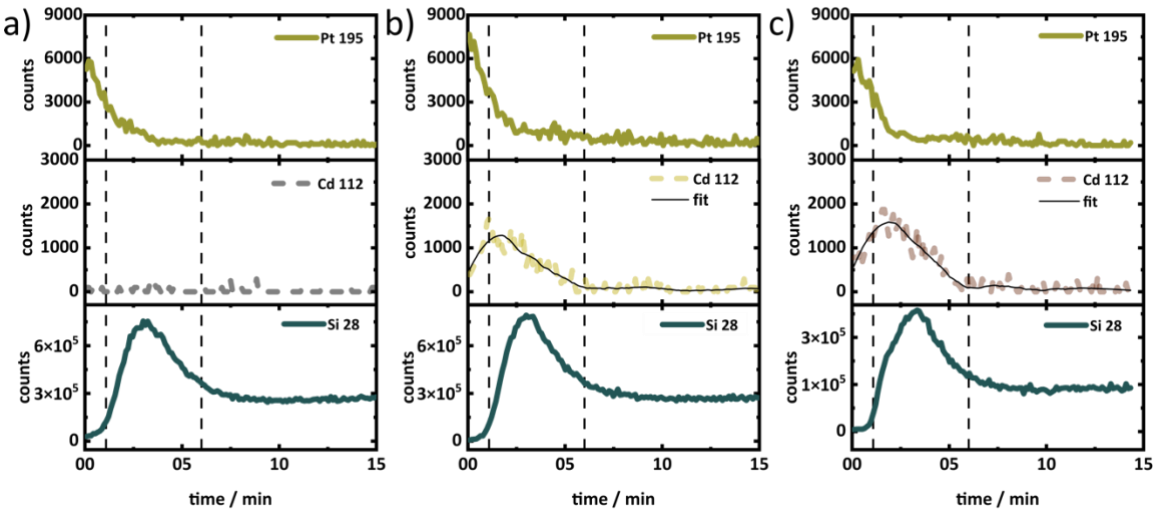

Figure 9: SIMS results of (a) drop casted and untreated, (b) drop casted and solvent treatment and (c) soaked for 24 h, porous silica layers of 30 nm pore size. The panels from top to bottom correspond to Pt, Cd and Si concentration. The dashed line at 1 min indicates the position of the top of the porous structure (Pt signal disappears). The second dashed line (6 min) corresponds to the end of porous silica layer which is determined from the end point of the intense signal of Si species. After that, the signal of Si is from the non-porous Si wafers.

To summarize, we have shown the successful infiltration of pre-synthesized CdSe QDs into porous silica of 10 nm and 30 nm pore sizes. It was observed that due to higher pore volume 30 nm porous silica shows higher loading after treatment than 10 nm porous silica matrix. This can be related to a better accessibility of the pores with higher pore size. The amount of infiltrated QDs can be influenced via drop casting of additional solvent on a pre drop casted porous matrix as well as via varying the soaking time of a porous matrix in a QD solution. Via this method, a porous thin film matrix can be doped with luminescent QDs which keep their luminescent properties upon deposition. This cannot be achieved via the SILAR process, which is lacking controllability over nanocrystal quality and size distribution.

Supplementary Materials: Figure S1: Top view SEM images and cross section SEM images of the porous layers; Figure S2: TEM image and size distribution analysis of CdSe QDs; Figure S3: Raw absorption spectra of QDs infiltrated porous silica layers; Figure S4: absorption spectra of untreated porous silica layers; Figure S5: Absorption spectra & photoluminescence spectra of porous layers after 0.5 h and 2 h soaking in a QD solution; Figure S6: Photoluminescence decay traces; Figure S7: SEM images of untreated and treated (infiltration methods) porous silica layers; Figure S8: SEM images of untreated and treated (SILAR immersions) porous silica layers; Figure S9: SIMS depth profiles of untreated and treated (infiltration methods) porous silica layers of 10 nm pore size; Figure S10: Absorption spectra of glass substrate soaked in a solution of pre-synthesized CdSe QDs; Table S1: Fitting parameters photoluminescence decays

Author Contributions: Conceptualization, M.W., and A.S.; methodology, M.W., A.S., and R.B.; validation, R.B., and M.W.; formal analysis, R.B.; investigation, R.B., M.D. (Munira Dilshad), M.D. (Marco Diegel), J.D., J.P., and A.U.; resources, M.W.; data curation, R.B., and M.W.; writing—original draft preparation, R.B.; writing—review and editing, R.B., M.D. (Marco Diegel), J.D., J.P., A.U., A.S., and M.W.; visualization, R.B.; supervision, M.W.; project administration, M.W.; funding acquisition, M.W. All authors have read and agreed to the published version of the manuscript.

Funding: This work was financially supported by the German Research Foundation (DFG) under the Project No. 398816777 – CRC 1375 (NOA, C04 and B03). The EDX and XRD facilities are partially supported by European Fond for Regional Development (EFRE) under the Project No. FKZ 2023 HSB 0025. Financial support by the German Research Foundation (DFG) within the infrastructure grant 390918228–INST 275/391-1 (A.U.) is acknowledged.

Data Availability Statement: The original contributions presented in the study are included in the article/supplementary material, further inquiries can be directed to the corresponding author.

Acknowledgments: We are grateful to Uwe Brückner (Leibniz IPHT) for the SIMS measurements.

Conflicts of Interest: The authors declare no conflicts of interest.

References

1. Koole, R.; Groeneveld, E.; Vanmaekelbergh, D.; Meijerink, A.; de Mello Donegá, C. Size Effects on Semiconductor Nanoparticles. In *Nanoparticles: Workhorses of Nanoscience*, de Mello Donegá, C., Ed.; Springer Berlin Heidelberg: Berlin, Heidelberg, 2014; pp. 13-51.
2. Bawendi, M.G.; Steigerwald, M.L.; Brus, L.E. The Quantum-Mechanics of Larger Semiconductor Clusters (Quantum Dots). *Annu. Rev. Phys. Chem.* **1990**, *41*, 477-496.
3. Ekimov, A.I.; Efros, A.L.; Onushchenko, A.A. Quantum Size Effect in Semiconductor Microcrystals. *Solid State Commun.* **1985**, *56*, 921-924.
4. Shu, Y.; Lin, X.; Qin, H.; Hu, Z.; Jin, Y.; Peng, X. Quantum Dots for Display Applications. *Angew. Chem.* **2020**, *59*, 22312-22323.
5. Singh, V.; Priyanka; More, P.V.; Hemmer, E.; Mishra, Y.K.; Khanna, P.K. Magic-sized CdSe nanoclusters: a review on synthesis, properties and white light potential. *Mater. Adv.* **2021**, *2*, 1204-1228.
6. Shirasaki, Y.; Supran, G.J.; Bawendi, M.G.; Bulovic, V. Emergence of colloidal quantum-dot light-emitting technologies. *Nat. Photonics* **2013**, *7*, 13-23.
7. Zhou, J.; Liu, Y.; Tang, J.; Tang, W.H. Surface ligands engineering of semiconductor quantum dots for chemosensory and biological applications. *Mater. Today* **2017**, *20*, 360-376.
8. Silvi, S.; Credi, A. Luminescent sensors based on quantum dot–molecule conjugates. *Chem. Soc. Rev.* **2015**, *44*, 4275-4289.
9. Shamirian, A.; Ghai, A.; Snee, P.T. QD-Based FRET Probes at a Glance. *Sensors (Basel)* **2015**, *15*, 13028-13051.
10. Xiang, X.L.; Wang, L.X.; Zhang, J.J.; Cheng, B.; Yu, J.G.; Macyk, W. Cadmium Chalcogenide (CdS, CdSe, CdTe) Quantum Dots for Solar-to-Fuel Conversion. *Adv. Photonics Res.* **2022**, *3*.
11. Li, X.B.; Tung, C.H.; Wu, L.Z. Semiconducting quantum dots for artificial photosynthesis. *Nat. Rev. Chem.* **2018**, *2*, 160-173.

12. Holmes, M.A.; Townsend, T.K.; Osterloh, F.E. Quantum confinement controlled photocatalytic water splitting by suspended CdSe nanocrystals. *Chem. Commun.* **2012**, *48*, 371-373.
13. Murray, C.B.; Norris, D.J.; Bawendi, M.G. Synthesis and characterization of nearly monodisperse CdE (E = sulfur, selenium, tellurium) semiconductor nanocrystallites. *J. Am. Chem. Soc.* **1993**, *115*, 8706-8715.
14. Chang, J.; Waclawik, E.R. Colloidal semiconductor nanocrystals: controlled synthesis and surface chemistry in organic media. *RSC Adv.* **2014**, *4*, 23505-23527.
15. Yin, Y.; Alivisatos, A.P. Colloidal nanocrystal synthesis and the organic-inorganic interface. *Nature* **2005**, *437*, 664-670.
16. Peterson, M.D.; Cass, L.C.; Harris, R.D.; Edme, K.; Sung, K.; Weiss, E.A. The Role of Ligands in Determining the Exciton Relaxation Dynamics in Semiconductor Quantum Dots. *Annu. Rev. Phys. Chem.* **2014**, *65*, 317-339.
17. Lim, S.J.; Ma, L.; Schleife, A.; Smith, A.M. Quantum dot surface engineering: Toward inert fluorophores with compact size and bright, stable emission. *Coord. Chem. Rev.* **2016**, *320*, 216-237.
18. Hartley, C.L.; Kessler, M.L.; Dempsey, J.L. Molecular-Level Insight into Semiconductor Nanocrystal Surfaces. *J. Am. Chem. Soc.* **2021**, *143*, 1251-1266.
19. Chen, Y.J.; Yu, S.; Fan, X.B.; Wu, L.Z.; Zhou, Y. Mechanistic insights into the influence of surface ligands on quantum dots for photocatalysis. *J. Mater. Chem. A* **2023**, *11*, 8497-8514.
20. Micheel, M.; Baruah, R.; Kumar, K.; Wächtler, M. Assembly, Properties, and Application of Ordered Group II-VI and IV-VI Colloidal Semiconductor Nanoparticle Films. *Adv. Mater. Interfaces* **2022**, *9*.
21. Boles, M.A.; Engel, M.; Talapin, D.V. Self-Assembly of Colloidal Nanocrystals: From Intricate Structures to Functional Materials. *Chem. Rev.* **2016**, *116*, 11220-11289.
22. Rogach, A.L.; Gaponik, N.; Lupton, J.M.; Bertoni, C.; Gallardo, D.E.; Dunn, S.; Li Pira, N.; Paderi, M.; Repetto, P.; Romanov, S.G.; et al. Light-Emitting Diodes with Semiconductor Nanocrystals. *Angew. Chem.* **2008**, *47*, 6538-6549.
23. Wood, V.; Bulovic, V. Colloidal quantum dot light-emitting devices. *Nano Rev.* **2010**, *1*, 5202.
24. Semonin, O.E.; Luther, J.M.; Beard, M.C. Quantum dots for next-generation photovoltaics. *Mater. Today* **2012**, *15*, 508-515.
25. Tang, J.A.; Sargent, E.H. Infrared Colloidal Quantum Dots for Photovoltaics: Fundamentals and Recent Progress. *Adv. Mater.* **2011**, *23*, 12-29.
26. Liu, Z.K.; Yuan, J.Y.; Hawks, S.A.; Shi, G.Z.; Lee, S.T.; Ma, W.L. Photovoltaic Devices Based on Colloidal PbX Quantum Dots: Progress and Prospects. *Sol. RRL* **2017**, *1*, 1600021.
27. Jin, L.; Zhao, H.G.; Wang, Z.M.M.; Rosei, F. Quantum Dots-Based Photoelectrochemical Hydrogen Evolution from Water Splitting. *Adv. Energy Mater.* **2021**, *11*, 2003233.
28. Qureshi, A.; Shaikh, T.; Niazi, J.H. Semiconductor quantum dots in photoelectrochemical sensors from fabrication to biosensing applications. *Analyst* **2023**, *148*, 1633-1652.
29. Li, N.; Mahalingavelar, P.; Vella, J.H.; Leem, D.S.; Azoulay, J.D.; Ng, T.N. Solution-processable infrared photodetectors: Materials, device physics and applications. *Mater. Sci. Eng. R Rep.* **2021**, *146*.
30. Besson, S.; Gacoin, T.; Ricolleau, C.; Jacquiod, C.; Boilot, J.P. 3D quantum dot lattice inside mesoporous silica films. *Nano Lett.* **2002**, *2*, 409-414.

31. Demchyshyn, S.; Roemer, J.M.; Groiss, H.; Heilbrunner, H.; Ulbricht, C.; Apaydin, D.; Böhm, A.; Rütt, U.; Bertram, F.; Hesser, G.; et al. Confining metal-halide perovskites in nanoporous thin films. *Sci. Adv.* **2017**, *3*, e1700738.
32. Li, J.S.; Tang, Y.; Li, Z.T.; Ding, X.R.; Yu, B.H.; Lin, L.W. Largely Enhancing Luminous Efficacy, Color-Conversion Efficiency, and Stability for Quantum-Dot White LEDs Using the Two-Dimensional Hexagonal Pore Structure of SBA-15 Mesoporous Particles. *ACS Appl. Mater. Interfaces* **2019**, *11*, 18808-18816.
33. Wang, H.C.; Lin, S.Y.; Tang, A.C.; Singh, B.P.; Tong, H.C.; Chen, C.Y.; Lee, Y.C.; Tsai, T.L.; Liu, R.S. Mesoporous Silica Particles Integrated with All-Inorganic CsPbBr3 Perovskite Quantum-Dot Nanocomposites (MP-PQDs) with High Stability and Wide Color Gamut Used for Backlight Display. *Angew. Chem.* **2016**, *55*, 7924-7929.
34. Li, J.S.; Tang, Y.; Li, Z.T.; Li, J.X.; Ding, X.R.; Yu, B.H.; Yu, S.D.; Ou, J.Z.; Kuo, H.C. Toward 200 Lumens per Watt of Quantum-Dot White-Light-Emitting Diodes by Reducing Reabsorption Loss. *ACS Nano* **2021**, *15*, 550-562.
35. Fan, M.; Huang, J.P.; Turyanska, L.; Bian, Z.F.; Wang, L.C.; Xu, C.Y.; Liu, N.; Li, H.B.; Zhang, X.Y.; Zhang, C.X.; et al. Efficient All-Perovskite White Light-Emitting Diodes Made of In Situ Grown Perovskite-Mesoporous Silica Nanocomposites. *Adv. Funct. Mater.* **2023**, *33*.
36. Ren, H.; Li, Y.M.; Li, W.J.; Zhai, Q.C.; Cheng, L. Lead-halide perovskite quantum dots embedded in mesoporous silica as heterogeneous photocatalysts combined with organocatalysts for asymmetric catalysis. *Green Chem.* **2024**, *26*, 6068-6077.
37. Wang, T.Q.; Tian, B.B.; Han, B.; Ma, D.R.; Sun, M.Z.; Hanif, A.; Xia, D.H.; Shang, J. Recent Advances on Porous Materials for Synergetic Adsorption and Photocatalysis. *Energy Environ. Mater.* **2022**, *5*, 711-730.
38. Meng, L.; Zhao, F.Y.; Zhang, J.B.; Luo, R.X.; Chen, A.F.; Sun, L.N.; Bai, S.L.; Tang, G.S.; Lin, Y. Preparation of monodispersed PbS quantum dots on nanoporous semiconductor thin film by two-phase method. *J. Alloys Compd.* **2014**, *595*, 51-54.
39. Wang, P.; Zhu, Y.H.; Yang, X.L.; Li, C.Z.; Du, H.L. Synthesis of CdSe nanoparticles into the pores of mesoporous silica microspheres. *Acta Mater.* **2008**, *56*, 1144-1150.
40. Gao, X.H.; Nie, S.M. Doping mesoporous materials with multicolor quantum dots. *J. Phys. Chem. B* **2003**, *107*, 11575-11578.
41. Calvo, M.E.; Hidalgo, N.; Schierholz, R.; Kovács, A.; Fernández, A.; Bellino, M.G.; Soler-Illia, G.J.A.A.; Míguez, H. Full solution processed mesostructured optical resonators integrating colloidal semiconductor quantum dots. *Nanoscale* **2015**, *7*, 16583-16589.
42. Ghazaryan, L.; Kley, E.B.; Tünnermann, A.; Szeghalmi, A. Nanoporous SiO2 thin films made by atomic layer deposition and atomic etching. *Nanotechnology* **2016**, *27*, 255603.
43. Pérez-Anguiano, O.; Wenger, B.; Pugin, R.; Hofmann, H.; Scolan, E. Controlling Mesopore Size and Processability of Transparent Enzyme-Loaded Silica Films for Biosensing Applications. *ACS Appl. Mater. Interfaces* **2015**, *7*, 2960-2971.
44. Raman, N.K.; Anderson, M.T.; Brinker, C.J. Template-based approaches to the preparation of amorphous, nanoporous silicas. *Chem. Mater.* **1996**, *8*, 1682-1701.
45. Liu, Y.; Ren, W.; Zhang, L.Y.; Yao, X. New method for making porous SiO2 thin films. *Thin Solid Films* **1999**, *353*, 124-128.
46. Amirav, L.; Alivisatos, A.P. Photocatalytic Hydrogen Production with Tunable Nanorod Heterostructures. *J. Phys. Chem. Lett.* **2010**, *1*, 1051-1054.
47. Carbone, L.; Nobile, C.; De Giorgi, M.; Sala, F.D.; Morello, G.; Pompa, P.; Hytch, M.; Snoeck, E.; Fiore, A.; Franchini, I.R.; et al. Synthesis and micrometer-scale

assembly of colloidal CdSe/CdS nanorods prepared by a seeded growth approach. *Nano Lett.* **2007**, *7*, 2942-2950.
48. Sankapal, B.R.; Salunkhe, D.B.; Majumder, S.; Dubal, D.P. Solution-processed CdS quantum dots on TiO2: light-induced electrochemical properties. *RSC Adv.* **2016**, *6*, 83175-83184.
49. Schneider, C.A.; Rasband, W.S.; Eliceiri, K.W. NIH Image to ImageJ: 25 years of image analysis. *Nat Methods* **2012**, *9*, 671-675.
50. Norris, D.J.; Bawendi, M.G. Measurement and assignment of the size-dependent optical spectrum in CdSe quantum dots. *Phys. Rev. B* **1996**, *53*, 16338-16346.
51. Deng, Z.T.; Cao, L.; Tang, F.Q.; Zou, B.S. A new route to zinc-blende CdSe nanocrystals: Mechanism and synthesis. *J. Phys. Chem. B* **2005**, *109*, 16671-16675.
52. Hu, X.G.; Zrazhevskiy, P.; Gao, X.H. Encapsulation of Single Quantum Dots with Mesoporous Silica. *Ann Biomed Eng* **2009**, *37*, 1960-1966.
53. Abdelhady, A.L.; Afzaal, M.; Malik, M.A.; O'Brien, P. Flow reactor synthesis of CdSe, CdS, CdSe/CdS and CdSeS nanoparticles from single molecular precursor(s). *J. Mater. Chem.* **2011**, *21*, 18768-18775.
54. W. William Yu, L.Q., Wenzhuo Guo, and Xiaogang Peng. Experimental Determination of the Extinction Coefficient of CdTe, CdSe, and CdS Nanocrystals. *Chem. Mater.* **2003**, *15*, 2854-2860.
55. Crooker, S.A.; Hollingsworth, J.A.; Tretiak, S.; Klimov, V.I. Spectrally resolved dynamics of energy transfer in quantum-dot assemblies: Towards engineered energy flows in artificial materials. *Phys. Rev. Lett.* **2002**, *89*.
56. Kagan, C.R.; Murray, C.B.; Bawendi, M.G. Long-range resonance transfer of electronic excitations in close-packed CdSe quantum-dot solids. *Phys. Rev. B* **1996**, *54*, 8633-8643.
57. Akselrod, G.M.; Prins, F.; Poulikakos, L.V.; Lee, E.M.Y.; Weidman, M.C.; Mork, A.J.; Willard, A.P.; Bulovic, V.; Tisdale, W.A. Subdiffusive Exciton Transport in Quantum Dot Solids. *Nano Lett.* **2014**, *14*, 3556-3562.